PERGAMON

International Journal of Heat and Mass Transfer 44 (2001) 3833–3842

International Journal of HEAT and MASS TRANSFER

www.elsevier.com/locate/ijhmt

High Schmidt number mass transfer using Chapman–Kuhn's near wall coherent structure model

Mingyong Chen, Qian Chen, Jiang Zhe, Vijay Modi *

Department of Mechanical Engineering, Columbia University, 500 West 120th Street, Mail Code 4703, New York, NY 10027, USA

Received 8 September 2000; received in revised form 2 January 2001

Abstract

High Schmidt number mass transfer in a fully developed turbulent flow is examined using a near wall coherent structure model. The computational approach relies on specification of idealized boundary conditions in the form of a two eddy structure imposed at a distance of $y^+ = 40$ away from the wall. The parameters describing the spatial and temporal eddy behavior are obtained from a combination of experimental observation, analysis and computer trials as described by D.R. Chapman, G.D. Kuhn (AIAA Paper 81-1024 (1981) 306–316). Among these parameters, those describing the root mean square (rms) velocities in normal and spanwise directions are found to have significant influence on mass transfer at the wall. A correlation relating the mass transfer rate and the rms velocities is obtained. The effects of turbulence intensity on eddy viscosity and eddy diffusivity are also determined.

Keywords: High Schmidt number; Near wall model; Coherent structure; Mass transfer

1. Introduction

Electrochemical deposition and/or etching for the fabrication of magnetic and MEMS devices, metallic mechanical structures and more recently for copper metallization technology is frequently carried out under turbulent flow conditions. In general the transport of reactants, which can be charged, is carried out by three different mechanisms: convection, diffusion and electrical migration. The limiting case where the migration term is negligible (when a supporting electrolyte is present) and the concentration term at the electrode becomes zero (when operating at the mass transfer limited current plateau) is nevertheless important. Under these limiting conditions the transport equations reduce to a high Schmidt number convection–diffusion problem. This limit remains a valuable idealization since it permits the examination of fluid flow effects in electrochemical systems. In advanced electronics applications in particular, an understanding of these effects is important for achieving feature-scale (sub-micron to tens of microns) deposition uniformity in reactor systems that need to accommodate wafers as large as 0.30 m. The reactor scale flow is frequently turbulent, e.g., in a fountain plater with impinging jets of $\sim 10^{-2}$ m nozzle diameter and nozzle exit velocities of $\sim$1 m/s, the Reynolds numbers are $O(10^4)$.

In modeling turbulent flows the contribution of eddy viscosity to the total (eddy plus molecular) viscosity is found to be negligible at distances from the wall that are less than about 4–5 in wall units [2]. Heat transfer at $Pr \sim O(1)$ shows similar behavior, where the contribution of the turbulent eddy thermal diffusivity to the total diffusivity also becomes negligible within such a distance from the wall. Hence, the presence of roughness elements or structures within this region does not lead to deviations from flush surface analysis. At high Schmidt numbers of $O(10^3)$, however, the contributions of turbulence to the total diffusivity do not become negligible (say 10%) until a distance of about $y^+ = 0.4$–0.5 from the wall is reached (estimated using pipe wall data [3]). This distance corresponds to $O(1\ \mu m)$ in a $Re \sim O(10^4)$ turbulent flow with liquid water properties. Since feature

* Corresponding author. Tel.: +1-212-854-2956; fax: +1-212-854-3304.

E-mail address: modi@columbia.edu (V. Modi).

0017-9310/01/$ - see front matter
PII: S0017-9310(01)00034-5

Nomenclature

c	dimensionless concentration of chemical species
D	diffusion coefficient, m^2/s
D_t	eddy diffusivity, m^2/s
F	body force associated with the global pressure gradient, N
I	turbulence intensity in pipe flow
k	mass transfer coefficient, m/s
K^+	dimensionless mass transfer coefficient, $K^+ = k/u_\tau$
n	frequency, 1/s
n_1^+	dimensionless frequency of the SSE in Eq. (2)
n_{u2}^+	dimensionless frequency of the LSE in Eq. (2)
p	pressure, N/m^2
Sc	Schmidt number, $Sc = \nu/D$
Sc_t	turbulent Schmidt number, defined in Eq. (8)
t	time, s
T	maximum dimensionless period of the LSE, defined as $T = 4\pi/n_{u2}^+$
u	velocity in x-direction, m/s
u_τ	friction velocity on the wall defined as $\sqrt{\tau_w/\rho}$, m/s
v	velocity in y-direction, m/s
w	velocity in z-direction, m/s
x	streamwise distance, m
y	vertical or normal distance, m
z	spanwise distance, m

Greek symbols

α	dimensionless rms velocity in the x-direction at $y^+ = y_e^+$
α_1	constant in Eq. (2), $\alpha_1 = 0.45\alpha$
β	dimensionless rms velocity in the y-direction at $y^+ = y_e^+$
γ	dimensionless rms velocity in the z-direction at $y^+ = y_e^+$
ζ	dimensionless spanwise distance in Eq. (2), $\zeta = 2\pi z^+/z_{max}^+$
ν	kinematic viscosity, m^2/s
ν_t	turbulent eddy viscosity, m^2/s
ρ	density, kg/m^3
τ_w	shear stress on the wall, N/m^2
ϕ_{u2}	phase angle in Eq. (2)
ϕ_w	phase angle in Eq. (2)
ϕ_{w2}	phase angle in Eq. (2)

Subscripts

e	edge of the near wall region ($y^+ = 40$ in the present computations)
t	turbulent
w	wall

Superscripts

+	wall unit
−	mean
′	fluctuation

sizes of interest are of this order, if one is interested in the spatial distribution of mass transfer over such a feature it would be necessary to account for the interaction of these features with the flow in order to estimate the contribution of the species eddy diffusivity. It would seem then that only a complete direct numerical simulation (DNS) over a computational domain consisting of the entire reactor that resolves all the scales from the feature to the reactor scale would be required. Computationally however, DNS is feasible only at moderate Re and moderate Sc since the number of mesh points needed would be of the order of $Sc\,Re^{9/4}$. This estimate is based on an estimate of $O(Re^{9/4})$ points for the fluid flow [4] and the fact that the concentration layer is thinner than the hydrodynamic layer by $O(Sc^{1/3})$.

An alternate approach is adopted here where analysis is restricted to a region near the wall. In this region the turbulent flow displays a combination of organized coherent structures and apparently disorganized structures. In this wall region corresponding to $y^+ \leqslant 40$, coherent structures account for over 80% of the energy in the turbulent fluctuations [5]. Moreover at high Schmidt numbers, the concentration changes are well within this wall region for boundary layer flows.

It is generally accepted that the Reynolds stress and production of turbulence in the wall region are associated with quasi-periodic eddies, elongated in the flow direction and occurring in counter-rotating pairs separated by a distance of about 50 wall units. A schematic diagram of flow in the near wall region is shown in Fig. 1(a). Several investigators have carried out laboratory measurements of turbulent flow in the wall region. These measurements include, velocity gradients at the wall [6,7], scaling of wall region eddies [8,9], streamwise velocity field [10,11], spanwise velocity field [12], and temporal phase relations [13].

The early effort in computing the flow field in the near wall region using experimentally observed streamwise eddies to describe the boundary conditions at the edge of the wall region dates back to 1970s. Studies by Fortuna [14], Sirkar and Hanratty [15] and Hatziavramidis and Hanratty [16] rely on the specification of a time-dependent velocity field at the edge of the near wall region ($y^+ = 30$–40). The time-dependent Navier–

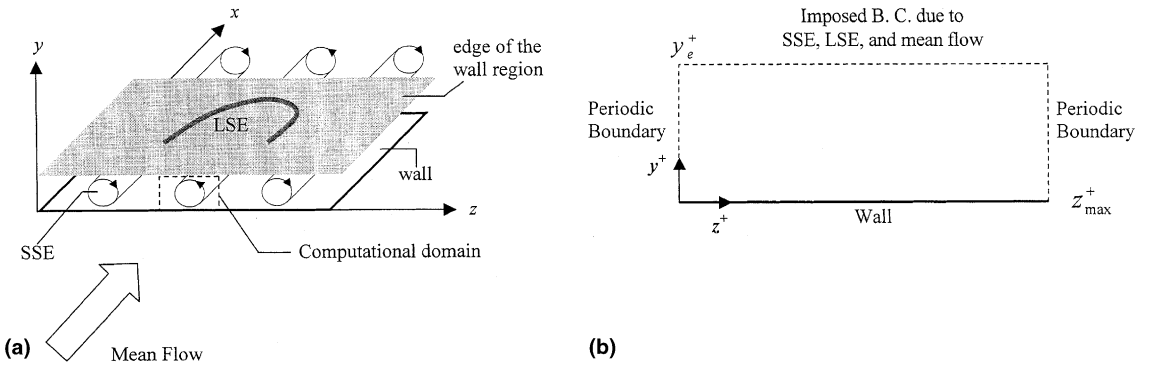

Fig. 1. (a) Schematic diagram of flow in the near wall region; (b) computational domain in present simulations.

Stokes equation in the wall region ($y^+ = 30$–40) is solved assuming that the flow is homogeneous in the streamwise direction and hence the momentum equation in the streamwise direction can be uncoupled with the normal and spanwise directions. The computed velocity fluctuations did show qualitative agreement with experimental data [17]. To obtain better quantitative agreement two separate studies by Chapman and Kuhn [1] and Nikolaides [18] reexamined the boundary condition at the edge of the wall region. Nikolaides reformulated the boundary condition to represent the flow due to two eddies of different spanwise scales ($z^+_{max} = 100$ and 400). An alternate formulation by Chapman and Kuhn [1] (designated CK81 here) used small-scale-eddies (SSE) of spanwise scale $z^+ = 100$ and large-scale eddies (LSE) that are z-direction independent. Their computational results of mean velocities, turbulence fluctuations and Reynolds stress showed very good agreement with experimental data. Hanratty [19] gave a detailed review of the studies mentioned above. Chapman and Kuhn [20] proposed two additional models that introduced intermediate-scale-eddies (MSE) in addition to SSE and LSE at the top boundary but without any demonstrated improvement over the earlier two-eddy model in CK81.

In the present study the CK81 model is employed to describe the near wall ($y^+ < 40$) flow field. This flow field provides the basis to compute high Schmidt number mass transfer in the presence of features (roughly $y^+ < 4$) or on a flush surface since the concentration boundary layer lies well within this wall region. In the present paper mass transfer computations are carried out for the flush wall case where the streamwise velocity computation is decoupled from the equations for the normal and spanwise velocities, rendering the problem two-dimensional. The presence of features would necessitate a three-dimensional calculation making the problem computationally intensive but otherwise a straightforward extension of the present analysis. The fact that such a calculation would be restricted to the wall region would however make it tractable with existing parallel computers today, unlike a calculation encompassing the entire reactor domain with resolution down to the feature scale.

The study allows the examination of the effect of Schmidt number and turbulence intensity on mass transfer. The effect of turbulence intensity on eddy viscosity and eddy diffusivity is also determined. The motivation for examining the effect of turbulence intensity comes from earlier studies that report significant heat/mass transfer rate enhancement with turbulence intensity. Simonich and Bradshaw [21] conducted heat transfer measurements in an air boundary layer and found that heat transfer rate increases with increasing free-stream turbulence, by about five percent for each percent of rms intensity. Other studies that report enhanced mass transfer with turbulence intensity increase are those by Kestin and Wood [22], Kataoka et al. [23] and Subbaiah et al. [24]. In the present paper a quantitative determination of the effect of turbulence intensity for high Schmidt number mass transfer is carried out. A correlation relating the mass transfer rate and rms turbulence velocities is obtained based on the numerical simulations.

2. Methodology

In the present paper the two-eddy model described in CK81 forms the basis of determining the flow in the wall region. The parameters describing the spatial and temporal eddy behavior were obtained from a combination of experimental observation, analysis and computer trials. The following normalization is used to obtain dimensionless variables:

$$t^+ = \frac{tu_\tau^2}{\nu}, \quad p^+ = \frac{p-\bar{p}}{\tau_w} = \frac{\Delta p}{\tau_w}, \quad n^+ = \frac{n\nu}{u_\tau^2}, \quad u_i^+ = \frac{u_i}{u_\tau}, \quad x_i^+ = \frac{x_i u_\tau}{\nu}, \tag{1}$$

where u_τ is the friction velocity. The subscript $i = 1, 2, 3$ corresponds to the velocities (u, v, w) and co-ordinates (x, y, z).

Due to the fact that the length of the quasi-streamwise vortices is an order of magnitude larger than their diameter, the variation in streamwise direction is small and neglected in the calculation. The simulation is conducted in a plane normal to the streamwise flow as shown in Fig. 1(b) in a rectangular region $0 \leqslant y^+ \leqslant y_e^+$ and $0 \leqslant z^+ \leqslant z_{max}^+$ with $y_e^+ = 40$ and $z_{max}^+ = 100$. In the spanwise direction, at $z^+ = 0$ and $z^+ = z_{max}^+$, periodic boundary conditions are specified. At the wall $y^+ = 0$, no-slip conditions are imposed. At $y^+ = y_e^+$, boundary conditions representing the two coherent harmonic components of motion, the SSE and LSE, and the mean flow are specified

$$\left.\begin{array}{ll} \text{Component 1 (SSE)} & \text{Component 2 (LSE)} \\ u_e^+ = 2\alpha_1 \sin(n_1^+ t^+)\sin\zeta & +[2(\alpha^2-\alpha_1^2)]^{1/2}\sin(n_{u2}^+ t^+ + \phi_{u2}) \quad +\overline{u_e^+} \\ v_e^+ = -2\beta\sin(n_1^+ t^+)\sin\zeta & \\ w_e^+ = 2\beta\sin(n_1^+ t^+ + \phi_w)\cos\zeta & +[2(\gamma^2-\beta^2)]^{1/2}\sin(\tfrac{1}{2}n_{u2}^+ t^+ + \phi_{w2}) \end{array}\right\} \tag{2}$$

The base case parameter values are taken from CK81 to be: $\overline{u_e^+} = 14$, $\alpha = 2$, $\beta = 1$, $\gamma = 1.3$, $\alpha_1 = 0.45\alpha$, $\phi_{u2} = 0$, $\phi_w = \pi/2$, $\phi_{w2} = 2\pi/3$, $n_1^+ = n_{u2}^+ = 0.044$, and $\zeta = 2\pi z^+/z_{max}^+$. The above set of parameters represents a *local* description of the flow in this near wall model. This description consists of the mean flow, turbulent fluctuations, their phase relationships, their dominant frequencies and length scales. Since the parameters have been normalized by friction velocity, local shear is a parameter as well. Here α, β, and γ represent the dimensionless root mean square (rms) velocities at $y^+ = y_e^+$: $(\overline{u_e'^{+2}})^{1/2}$, $(\overline{v_e'^{+2}})^{1/2}$, and $(\overline{w_e'^{+2}})^{1/2}$, respectively. The streamwise mean velocity $\overline{u_e^+}$ is derived from the commonly believed law of the wall. The phase angle ϕ_w is obtained from the continuity equation whereas ϕ_{w2} is determined by computer trial to obtain as good a match as possible with the law of wall. The angle ϕ_{u2} is set to be zero since the solution is found to be insensitive to this parameter.

Among the above parameters, the rms velocities (α, β, γ) may vary with geometry, flow conditions, unsteadiness, and surface roughness, etc. The mean frequency n_{u2}^+ of LSE is dependent on the turbulent boundary layer thickness whereas the SSE frequency n_1^+ is experimentally observed to be relatively invariant. Changes of these parameters may have significant effects on the mass transfer rate. In the present calculations, effects of the rms velocities and eddy frequencies on mass transfer are investigated. Effect of the rms velocities is examined for five values of β (0.5, 0.75, 1.0, 1.25, and 1.5) with the values of α and γ equaling 2β and 1.3β. To examine sensitivity to eddy frequencies the frequencies of LSE and SSE are assumed to be equal for the purpose of simplicity. Two sets of frequency values $n_1^+ = n_{u2}^+ = 0.044$ and 0.044×4 are chosen for computations. While some investigators [19] have suggested the importance of the length scale of turbulence, the effect of variation of the spanwise length scale z_{max}^+ is not examined in the present study.

Based on the dimensionless variables in Eq. (1), the continuity and Navier–Stokes equations take the form

$$\begin{aligned} &\frac{\partial v^+}{\partial y^+} + \frac{\partial w^+}{\partial z^+} = 0, \\ &\frac{\partial u_i^+}{\partial t^+} + v^+\frac{\partial u_i^+}{\partial y^+} + w^+\frac{\partial u_i^+}{\partial z^+} \\ &\quad = -\frac{\partial p^+}{\partial x_i^+} - \frac{\partial \overline{p}^+}{\partial x_i^+} + F_i^+(t^+) + \frac{\partial^2 u_i^+}{\partial y^{+2}} + \frac{\partial^2 u_i^+}{\partial z^{+2}}. \end{aligned} \tag{3}$$

Note that the calculation of u^+ is de-coupled from the calculation of v^+ and w^+ in this formulation and hence the u^+ component can be solved as a scalar once v^+ and w^+ are obtained. In the above equations F_i^+ is a body force corresponding to a global pressure gradient associated with the LSE and is defined as, $F_1^+(t^+) = \partial u_{e2}^+/\partial t^+$, $F_2^+(t^+) = 0$, $F_3^+(t^+) = \partial w_{e2}^+/\partial t^+$. The quantities u_{e2}^+ and w_{e2}^+ are the LSE (Component 2 in Eq. (2)) velocity components in x- and z-direction at $y^+ = y_e^+$.

Once the fluid flow is obtained, the concentration field can be obtained by solving the unsteady mass transfer equation. An order-of-magnitude analysis performed by Sirkar and Hanratty [15] concluded that, compared to the spanwise direction, the convective and diffusive mass transfer in streamwise direction have little effect on the fully developed high Schmidt number mass transfer rate and hence is neglected in the present calculations. The mass transfer equation is

$$\frac{\partial c}{\partial t^+} + v^+\frac{\partial c}{\partial y^+} + w^+\frac{\partial c}{\partial z^+} = \frac{1}{Sc}\left(\frac{\partial^2 c}{\partial y^{+2}} + \frac{\partial^2 c}{\partial z^{+2}}\right). \tag{4}$$

The computational domain is the same as that for fluid flow. At $z^+ = 0$ and $z^+ = z_{max}^+$, periodic boundary conditions are specified. At the wall $y^+ = 0$, the concentration is set to zero and at $y^+ = y_e^+$, the bulk concentration $(c = 1)$ is assumed to prevail.

A 2-D time dependent SIMPLER algorithm [25] based code is utilized to carry out the fluid flow calculation. The mean pressure $\overline{p}$ is assumed to be function of x alone. Since the mean pressure gradient $(\partial\overline{p}^+/\partial x^+)$ has only a negligible effect on sublayer turbulence [1], it is set to be zero in all the present computations. A 2-D time dependent concentration solver is developed to solve mass transfer with given fluid flow. The time period in the computation is chosen to be the maximum cycle of the LSE $(T = 4\pi/n_{u2}^+)$.

The fluid flow calculation is carried out using a mesh size of 40×40 (in y- and z-direction) using 200 time steps per period. Due to the high Schmidt number, the

mass transfer calculation needs much finer grids than that for fluid flow. A mesh size of 150×90 (in y- and z-direction) is used for the mass transfer computation with the same time step as that for the flow. With a stretching factor of 1.05 in the normal direction the distance of the first point away from the wall for the mass transfer calculation is about twenty times smaller than that for the fluid flow calculation. Uniform mesh is used in the spanwise direction.

As the simulation progresses, the effect of initial conditions is found to gradually decay. Once a quasi-steady periodic solution is obtained, calculations are continued for two more periods to obtain fluid flow statistics. Once the fluid flow is obtained the known temporal velocity fields are stored and used to solve the mass transfer problem. Once the concentration field becomes periodic in the spanwise direction, data reduction in carried out by continuing the simulation for two time periods. One complete fluid flow calculation on a 40×40 grid (requiring about 2800 time steps to achieve quasi-steady periodic solution) needs about six hours and one case of mass transfer calculation on 150×90 grid (requiring about 4600 time steps to achieve quasi-steady periodic solution) needs about half an hour on a Pentium III 800 MHz with 512 MB of RAM.

The average velocities, rms velocities, Reynolds stress, and turbulent Schmidt number are calculated as follows:

$$\overline{u^+}_j = \frac{1}{N}\frac{1}{M}\sum_{n=1}^{N}\sum_{m=1}^{M} u^{+n}_{j,m}, \tag{5}$$

$$(\overline{u'^{+2}_j})^{1/2} = \sqrt{\frac{1}{NM-1}\sum_{n=1}^{N}\sum_{m=1}^{M}(u^{+n}_{j,m} - \overline{u^+}_j)^2}, \tag{6}$$

$$-\overline{u'^+v'^+}_j = -\frac{1}{NM-1}\sum_{n=1}^{N}\sum_{m=1}^{M}(u^{+n}_{j,m} - \overline{u^+}_j)(v^{+n}_{j,m} - \overline{v^+}_j), \tag{7}$$

$$Sc_t = \left(-\overline{u^{+\prime}v^{+\prime}}\right)\frac{\mathrm{d}\overline{c}}{\mathrm{d}y^+}\Big/(-\overline{c^{+\prime}v^{+\prime}})\frac{\mathrm{d}\overline{u^+}}{\mathrm{d}y^+}, \tag{8}$$

where N is the sampling rate in time period T, M is the sampling rate in spanwise direction and the subscript j is the index in y-direction. T is the maximum period of LSE ($T = 4\pi/n^+_{u2}$). The averaged concentration $\overline{c}$ and $-\overline{v'^+c'}$ can be computed similarly.

Computations with a finer grid (60×50) for the flow using 250 time steps per period are also carried out to verify adequacy of grid resolution. No observable difference is found between the simulation results using the two sets of grids and the results faithfully reproduce the $\overline{u}$, $(\overline{u'^2})^{1/2}$, $(\overline{v'^2})^{1/2}$, $(\overline{w'^2})^{1/2}$, and $-\overline{u'v'}$ distributions given in CK81. Hence only the streamwise mean velocity distribution in the normal direction is reported in this paper and is shown in Fig. 2. As noted in CK81, the simulation results show good agreement with experiments [26,27].

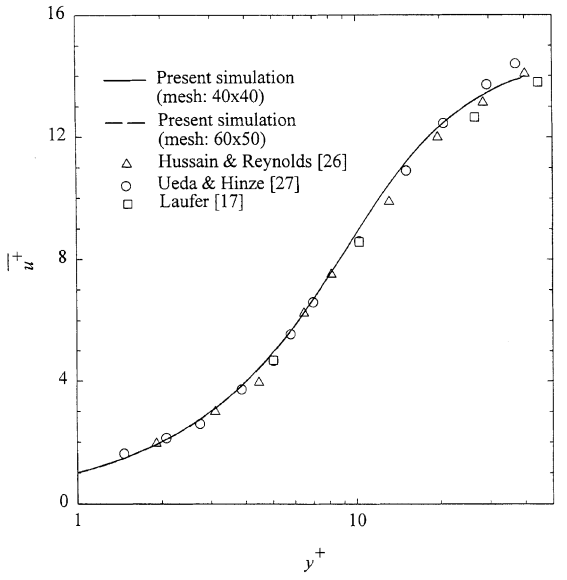

Fig. 2. Variation of streamwise mean velocity with normal distance from the wall.

To verify adequacy of grid resolution for the mass transfer calculations, the turbulent Schmidt number distribution in the wall-normal direction is obtained using three different grids (90×60, 150×90, 200×120). The corresponding time step per period for the three grids is 150, 200 and 250, respectively. The results are shown in Fig. 3. While the maximum relative error between the two finest grids is 7%, this discrepancy is limited to $y^+ < 0.5$. Everywhere else the agreement of Sc_t is considerably better.

3. Results and discussion

The variation of mean concentration $\overline{c}$ versus the wall-normal distance from the wall is plotted in Fig. 4 for Schmidt numbers of 900 and 2140. Experimental data of Flender and Hiby [28] and Lin et al. [29] are also shown in the figure. Note that in the region near the wall the experimental data are steeper than the present simulations approaching the bulk concentration at lower y^+ values. The concentration is seen to reach the bulk concentration value by $y^+ = 5$, well within the computational domain because of the high Schmidt numbers.

While it is generally accepted that the near wall behavior of turbulent eddy diffusivity is $\sim O(y^m)$ there has been considerable debate in the literature about the value of the exponent m, in particular whether it is 3 or 4 or perhaps an empirical value in between [30–32]. Shaw [33] obtained $D_t/\nu = 0.000463y^{+3.38}$ for mass transfer at

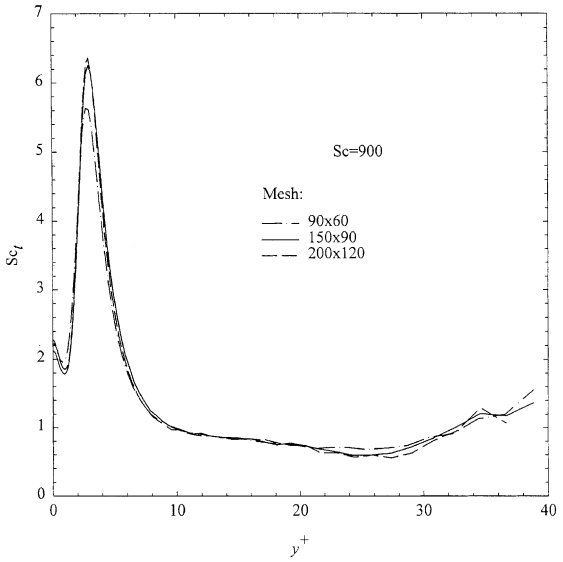

Fig. 3. Variation of turbulent Schmidt number with distance from the wall for three different mesh sizes ($Sc = 900$).

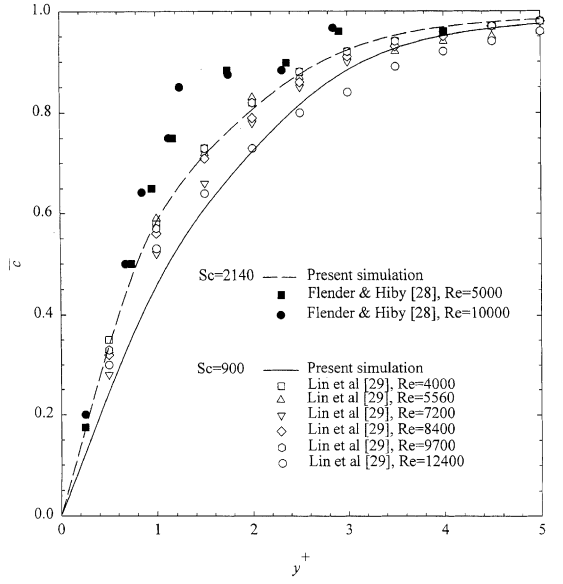

Fig. 4. Variation of the near-wall concentration with distance from the wall. Experimental data of Flender and Hiby [28] and Lin et al. [29] are also shown.

high Schmidt numbers. Recently Na and Hanratty [32] calculated D_t/v for high Schmidt number mass transfer using the Lagrangian calculation results of concentration field by Papavassiliou and Hanratty [34,35]. The present simulation results of D_t/v versus the normal distance are shown in Fig. 5 along with Na and Hanratty's calculated results and the prediction using Shaw's

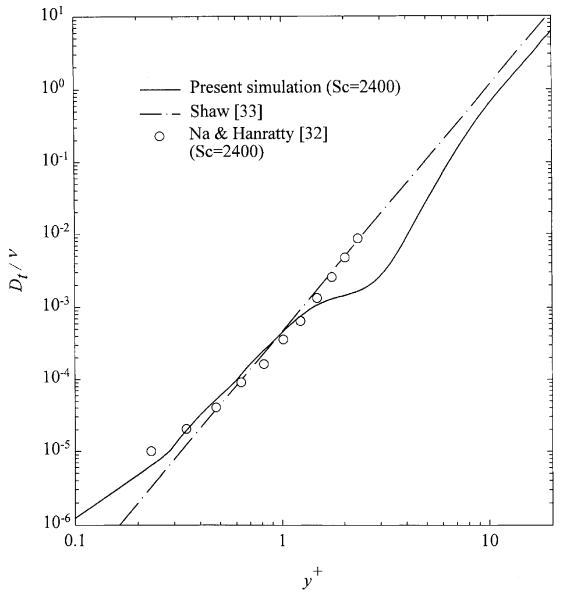

Fig. 5. Variation of D_t/v with distance from the wall. Results by Shaw [33] and Na and Hanratty [32] are also shown.

correlation. These results lie in the same region especially for the region $0.2 < y^+ < 1$. For $y^+ > 1$ the present simulation result is less than the other two.

For fully developed flow and mass transfer, the mass flux becomes constant and a dimensionless mass transfer coefficient, K^+ can be calculated as follows:

$$K^+ = \frac{1}{Sc}\left[\frac{d\bar{c}}{dy^+}\right]_w. \tag{9}$$

The mass transfer coefficient K^+ is shown as a function of Schmidt number in Fig. 6 along with the experiment-

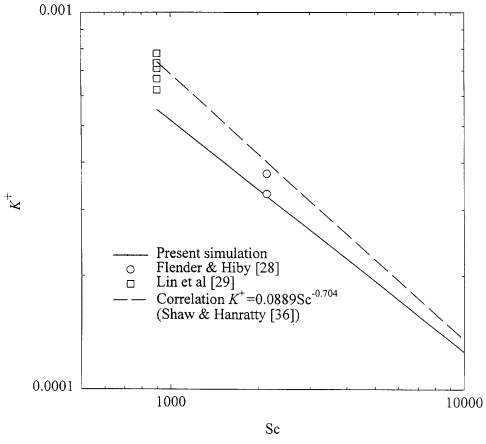

Fig. 6. Variation of mass transfer coefficient K^+ with Schmidt number along with experimental data [28,29] and correlation by Shaw and Hanratty [36].

based correlation by Shaw and Hanratty [36] ($K^+ = 0.0889Sc^{-0.704}$) and experimental data of Flender and Hiby [28] and Lin et al. [29]. The experimental data of Flender and Hiby [28] were obtained at two different Reynolds numbers: 5000 and 10 000. The Reynolds numbers in Lin et al. [29] study range from 4000 to 12 400. The experimental data lie between the results of the present simulation and Shaw and Hanratty's correlation, which is generally higher than the present simulation results. The Schmidt number dependence of the mass transfer coefficient is $K^+ \sim Sc^{-0.61}$ in the present simulations.

Most Reynolds Averaged Navier–Stokes or RANS based turbulence modeling efforts rely on a turbulent Schmidt number when solving the time-averaged mass transfer equation. The turbulent Schmidt numbers extracted from the present solutions using Eq. (8) are shown in Fig. 7 for $Sc = 900$–10 000. Available experimental data [37] and an algebraic formula for Sc_t [37] are also shown. For $y^+ > 6$, the present simulation results for high Sc are in the same range as the experimental data and predictions using the formula. Closer to the wall ($y^+ < 5$), however, the simulation results for Sc_t are much higher showing a peak around $y^+ \approx 3$, followed by a rapid drop off to a value of about 2 at the wall, which is roughly the same as that from Kays and Crawford's formula. The present simulations show that the peak value of Sc_t increases with the Schmidt numbers, whereas Sc_t at the wall slightly decreases with Schmidt number. If one were to obtain dc/dy from the experimental data shown in Fig. 4 and assume all other quantities in Eq. (8) to remain the same as in the present simulations, then the sharp peak in Sc_t around $y^+ = 3$ is no longer observed. Lacking any other means to validate the simulations for Sc_t in this region, further study would be needed to make definitive conclusions.

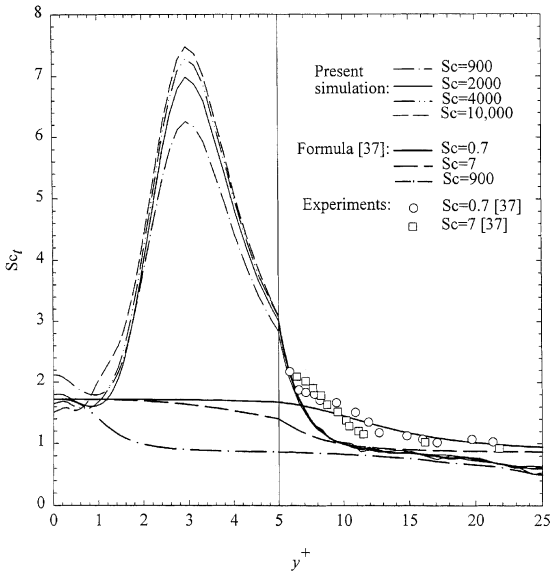

Fig. 7. Variation of turbulent Schmidt number with the distance from the wall for $Sc = 900$–10 000 along with experimental data and a suggested formula by Kays and Crawford [37].

In the existing literature there is a clear indication that rms turbulent intensity or velocity fluctuations do play a role in determining mass transfer even though there is no established quantitative relationship between the two. Heat transfer measurements by Simonich and Bradshaw [21] in an air boundary layer reveal that one percent increase of rms intensity can increase the heat transfer by about five percent. Kataoka et al. [23] experimentally studied high Schmidt number ($Sc = 1800$) mass transfer to a flat plate in an axisymmetric impinging turbulent jet flow. They compared their experimental mass transfer rates with their theoretical results obtained under turbulence-free conditions (free-stream turbulence intensity is zero), and found that the mass transfer to the plate was greatly enhanced owing to the existence of turbulent fluctuations in the wall region. Subbaiah et al. [24] in a study of mass transfer in an electrochemical cell observed that the presence of turbulence promoters increased the mass transfer rate by 110% in forced circulation flow in the range of promoters considered.

The two-eddy near wall model utilized in the present study provides a test-bed to examine the effect on mass transfer rate of the turbulence velocity fluctuations (α, β, γ) at the edge of the near wall region. Computations were carried out for five different values of β (0.5, 0.75, 1.0, 1.25, and 1.5) where $\beta = v_{rms}/u_\tau$ and v_{rms} is the dimensional y-direction rms velocity at $y^+ = y_e^+$. Both α and γ were also proportionally altered according to $\alpha = 2.0\beta$ and $\gamma = 1.3\beta$. Note however that changes in α do not alter fully developed mass transfer as seen from Eq. (4). All the other parameters are the same as the base case parameter values taken from CK81. Variation of the mass transfer rate at the wall with β is shown in Fig. 8. In this figure the mass transfer coefficient K^+ is normalized by $Sc^{-0.61}$ based on the simulations shown in Fig. 6. It is seen from Fig. 8 that higher values of β can lead to significant enhancement in mass transfer. A correlation obtained from the simulation results relating the mass transfer rate to the rms velocity β is given by

$$K^+ = (-0.0082\beta^2 + 0.0342\beta + 0.0097)Sc^{-0.61}. \quad (10)$$

As observed earlier β represents the normalized rms velocity at $y^+ = y_e^+$ in the wall-normal direction. In order to obtain some insight into the parameter β, we consider a fully developed pipe flow at a Reynolds number $Re = 10^4$ based on pipe diameter and average pipe flow velocity. The commonly used turbulence intensity I is defined as follows:

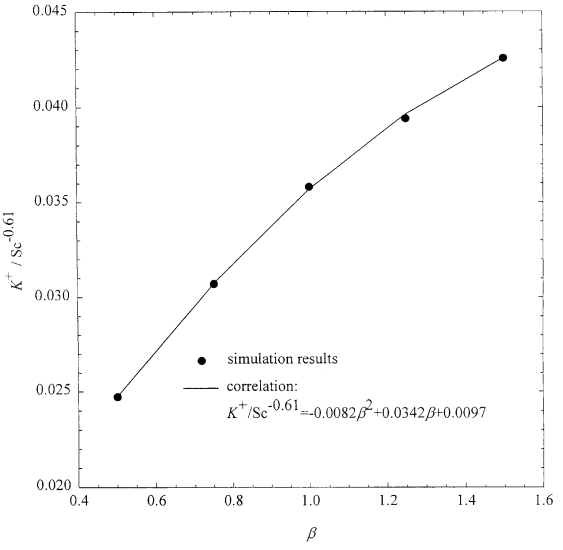

Fig. 8. Effect of normalized y-direction rms velocity β on mass transfer coefficient.

$$I = \frac{1}{U_{\mathrm{av}}}\sqrt{\frac{u_{\mathrm{rms}}^2 + v_{\mathrm{rms}}^2 + w_{\mathrm{rms}}^2}{3}}, \tag{11}$$

where U_{av} is the streamwise average velocity in the pipe flow and u_{rms}, v_{rms}, and w_{rms} are x-, y-, and z-direction rms velocities at $y^+ = 40$. If α and γ are assumed to change with β according to $\alpha = 2.0\beta$ and $\gamma = 1.3\beta$, an increase in β from 1.07 to 1.50 corresponds to an increase in I from 10% to 14%. Over such an increase in turbulence intensity I, the present results indicate a 15% increase in mass transfer.

The effect of changes in eddy frequencies (n_1^+, n_{u2}^+) is examined using a four-fold increase in the two values, i.e., $n_1^+ = n_{u2}^+ = 0.044$ and $n_1^+ = n_{u2}^+ = 0.044 \times 4$. Note that the SSE frequency n_1^+ and the LSE frequency n_{u2}^+ are set to be the same in order to simplify the computation. The other parameters were maintained the same as those in the base case. The numerical mass transfer rate at the wall (not shown here) was found to be insensitive to changes of eddy frequency (n_1^+, n_{u2}^+).

The turbulent eddy viscosity ν_t and eddy diffusivity D_t are two important quantities in traditional turbulence modeling approaches that utilize Reynolds averaged Navier–Stokes and concentration equations. Effects of β on ν_t/ν and D_t/ν are also studied in the present paper and the results are shown in Figs. 9 and 10, respectively. Increasing β generally increases both the turbulent eddy viscosity and eddy diffusivity. From Fig. 9 it can be seen that, the turbulence eddy viscosity ν_t is less than ten percent of the molecular viscosity ν when $y^+ < 5$. The turbulence eddy diffusivity D_t (as seen in Fig. 10 for $Sc = 900$) is not negligible compared to the molecular diffusivity D ($D_t/D \leqslant 10\%$ or $D_t/\nu \leqslant 10^{-4}$ for $Sc \sim 900$) until $y^+ < 0.5$. This suggests that for high Schmidt number mass transfer simulations the first grid point near the wall should be at least within $y^+ < 0.5$.

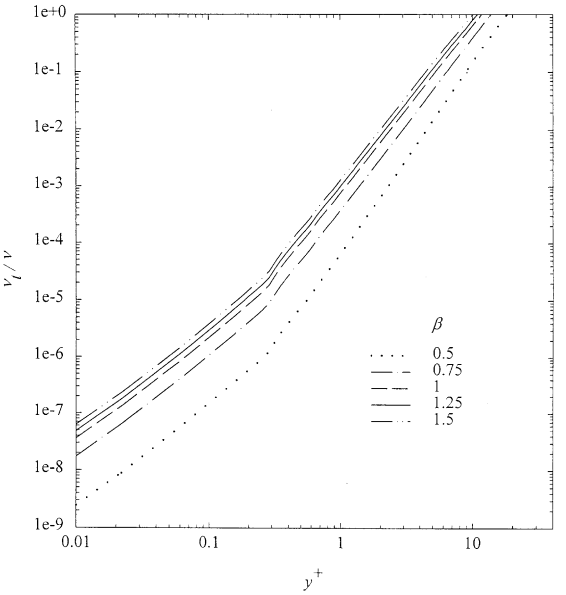

Fig. 9. Effect of normalized y-direction rms velocity β on the variation of ν_t/ν with y^+ ($\alpha = 2\beta$, $\gamma = 1.3\beta$ are assumed).

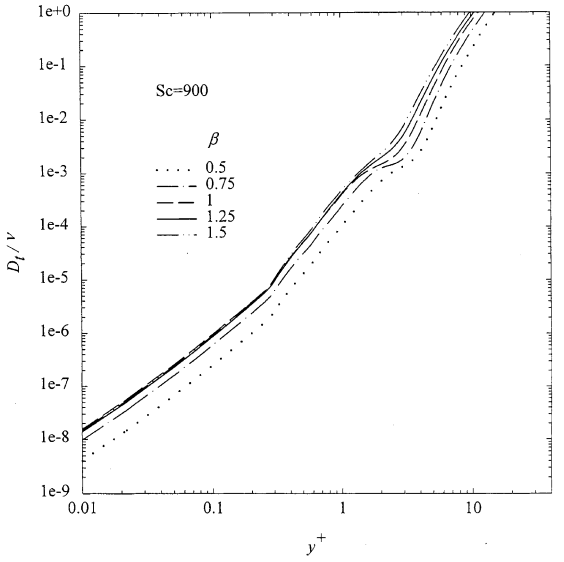

Fig. 10. Effect of normalized y-direction rms velocity β on the variation of D_t/ν with y^+ ($\gamma = 1.3\beta$ is assumed).

4. Conclusion

Using the two-eddy model of CK81, fully developed turbulent flow and high Schmidt number mass transfer

near a wall are simulated. These idealizations permit the use of two-dimensional simulations. This modeling approach can however be easily extended to a three-dimensional simulation, which would be necessary in the presence of features on the surface. The present two-dimensional simulations could be utilized to provide the upstream "fully-developed" flow boundary condition for the three-dimensional simulation. Although it is difficult to carry out such a three-dimensional calculation using a single CPU personal computer as was utilized in the present study, the existing parallel computers today can make this problem feasible due to the fact that such a calculation would be restricted to the wall region. Thus the approach presented here would make viable calculations that would otherwise be difficult with a full Direct Numerical Simulations approach. Even though the low-order model adopted here utilizes only two harmonic perturbations to simulate the near-wall turbulent coherent structure, the results show that we can reasonably retrieve some of the key statistics of turbulence critical to turbulent transport as well as mass transport, something that is very difficult with traditional turbulence modeling (k–ε or k–ω turbulence model).

The effect of turbulent velocity fluctuations on mass transfer rate K^+ is examined in the present paper. It is found that an increase in wall-normal turbulent velocity fluctuations (and an associated increase in the spanwise direction fluctuations) can considerably enhance the mass transfer rate. A correlation that relates K^+ to the normal direction rms velocity β is obtained from the numerical simulation results. Effects of the turbulent velocity fluctuations on the eddy viscosity and eddy diffusivity are also determined. A sensitivity study shows that the mass transfer rate is insensitive to the change in eddy frequencies.

The present approach allows the examination of the turbulent Schmidt number distribution in the region $y^+ \leqslant 5$ considerably closer to the wall than other numerical or experimental studies. The computed results show unusually high turbulent Schmidt numbers in this region. Further study is warranted to establish the validity of this behavior.

Acknowledgements

This work was partially supported by the National Science Foundation under the award CTS-97-06824.

References

[1] D.R. Chapman, G.D. Kuhn, Two-component Navier–Stokes computational model of viscous sublayer turbulence, AIAA Paper 81-1024 (1981) 306–316.

[2] F.M. White, in: Viscous Fluid Flow, McGraw-Hill, New York, 1974, p. 491.

[3] J.S. Newman, Electrochemical Systems, second ed., Prentice-Hall, Englewood Cliffs, NJ, 1991.

[4] J.H. Ferziger, M. Peric, Computational Methods for Fluid Dynamics, second ed., Springer, Berlin, 1999, pp. 259–260.

[5] J.L. Lumley, P. Blossey, The low dimensional approach to turbulence, in: M.D. Salas, J.N. Hefner, L. Sakell (Eds.), in: Modeling Complex Turbulent Flows, Kluwer Academic Publishers, Boston, 1999, pp. 89–106.

[6] T.J. Hanratty, J.A. Campbell, Measurements of wall shear stress, in: R.J. Goldstein (Ed.), in: Fluid Mechanics Measurements, Hemisphere, Washington, DC, 1983, p. 559.

[7] Z.X. Mao, T.J. Hanratty, The use of scalar transport probes to measure wall shear stress in a flow with imposed oscillations, Exp. Fluids 3 (1985) 129–135.

[8] J.E. Mitchell, T.J. Hanratty, A study of turbulence at a wall using an electrochemical wall shear-stress meter, J. Fluid Mech. 26 (part 1) (1966) 199–221.

[9] T.J. Hanratty, Study of turbulence close to a solid wall, Phys. Fluids Suppl. (1967) S126–S133.

[10] J.H.A. Hogenes, T.J. Hanratty, The use of multiple wall probes to identify coherent flow patterns in the viscous wall region, J. Fluid Mech. 124 (1982) 363–390.

[11] C. Nikolaides, K.K. Lau, T.J. Hanratty, A study of the spanwise structure of coherent eddies in the viscous wall region, J. Fluid Mech. 130 (1983) 91–108.

[12] C. Nikolaides, K.K. Lau, J.H.A. Hogenes, T.J. Hanratty, Structure of turbulence close to a solid, Ann. NY Acad. Sci. 44 (1983) 374–390.

[13] H.P. Kreplin, H. Eckelmann, Propagation of perturbations in the viscous sublayer and adjacent wall region, J. Fluid Mech. 95 (part 2) (1979) 305–322.

[14] G. Fortuna, Effect of drag-reducing polymers on flow near a wall, Ph.D. Thesis, University of Illinois, Urbana, IL, 1971.

[15] K.K. Sirkar, T.J. Hanratty, Relation of turbulent mass transfer to a wall at high Schmidt numbers to the velocity field, J. Fluid Mech. 44 (part 3) (1970) 589–603.

[16] D.T. Hatziavramidis, T.J. Hanratty, The representation of the viscous wall region by a regular eddy pattern, J. Fluid Mech. 95 (part 4) (1979) 655–679.

[17] J. Laufer, The structure of turbulence in fully developed pipe flow, in: NACA TN, 1954, p. 1174.

[18] C. Nikolaides, A study of the coherent structures in the viscous wall region of a turbulent flow, Ph.D. Thesis, University of Illinois, Urbana, IL, 1984.

[19] T.J. Hanratty, A conceptual model of the viscous wall region, in: S.J. Kline, N.H. Afgan (Eds.), in: Near-Wall Turbulence, Hemisphere, New York, 1988, pp. 81–103.

[20] D.R. Chapman, G.D. Kuhn, The limiting behavior of turbulence near a wall, J. Fluid Mech. 170 (1986) 265–292.

[21] J.C. Simonich, P. Bradshaw, Effect of free-stream turbulence on heat transfer through a turbulent boundary layer, J. Heat Transfer 100 (1978) 671–677.

[22] J. Kestin, R.T. Wood, The influence of turbulence on mass transfer from cylinders, J. Heat Transfer 93 (1971) 321–327.

[23] K. Kataoka, Y. Kamiyama, S. Hashimoto, T. Komai, Mass transfer between a plane surface and an impinging

turbulent jet: the influence of surface-pressure fluctuations, J. Fluid Mech. 119 (1982) 91–105.
[24] T. Subbaiah, P. Venkateswarlu, R.P. Das, G.J.V.J. Raju, Improved ionic mass transfer in an electrochemical cell in presence of turbulence promoters, Hydrometallurgy 42 (1996) 93–102.
[25] S.V. Patankar, Numerical Heat Transfer and Fluid Flow, Taylor & Francis, London, 1980.
[26] A.K.M.F. Hussain, W.C. Reynolds, Measurements in fully developed turbulent channel flow, J. Fluids Eng. – Trans. ASME 97 (4) (1975) 568–580.
[27] H. Ueda, J.O. Hinze, Fine-structure turbulence in the wall region of a turbulent boundary layer, J. Fluid Mech. 67 (part 1) (1975) 125–143.
[28] J.F. Flender, J.W. Hiby, Investigation of solid–liquid mass-transfer by means of a photometric measuring method, Chemie Ingenieur Technik 53 (5) (1981) 388–389.
[29] C.S. Lin, R.W. Moulton, G.L. Putnam, Mass transfer between solid wall and fluid streams, Ind. Eng. Chem. 3 (1953) 640.
[30] A.S. Monin, A.M. Yaglom, Statistical Fluid Mechanics; Mechanics of Turbulence, vol. 1, MIT Press, Cambridge, MA, 1971, pp. 343–347.
[31] J.S. Son, T.J. Hanratty, Limiting relation for the eddy diffusivity close to a wall, AIChE J. 13 (4) (1967) 689–696.
[32] Y. Na, T.J. Hanratty, Limiting behavior of turbulent scalar transport close to a wall, Int. J. Heat Mass Transfer 43 (2000) 1749–1758.
[33] D.A. Shaw, Mechanism of turbulent mass transfer to a pipe wall at high Schmidt number, Ph.D. Thesis, University of Illinois, Urbana, 1976.
[34] D. Papavassiliou, T.J. Hanratty, The use of Lagrangian methods to describe turbulent transport of heat from a wall, Ind. Eng. Chem. Res. 34 (1995) 3359–3367.
[35] D. Papavassiliou, T.J. Hanratty, Transport of a passive scalar in a turbulent channel flow, Int. J. Heat Mass Transfer 40 (6) (1997) 1303–1311.
[36] D.A. Shaw, T.J. Hanratty, Turbulent mass transfer rates to a wall for large Schmidt numbers, AIChE J. 23 (1977) 28–37.
[37] W.M. Kays, M.E. Crawford, Convective Heat and Mass Transfer, second ed., McGraw-Hill, New York, 1980, pp. 228–229.